



BNL-113926-2017-JA

Hydrothermal Growth of ZnO Nanowire Arrays: Fine Tuning By Precursor Supersaturation

D. Yan, J. Cen, W. Zhang, A. Orlov, M. Liu

Submitted to the Journal of CrystEngComm

December 2016

Center for Functional Nanomaterials

Brookhaven National Laboratory

**U.S. Department of Energy
USDOE Office of Science (SC),
Basic Energy Sciences (BES) (SC-22)**

Notice: This manuscript has been authored by employees of Brookhaven Science Associates, LLC under Contract No. DE- SC0012704 with the U.S. Department of Energy. The publisher by accepting the manuscript for publication acknowledges that the United States Government retains a non-exclusive, paid-up, irrevocable, world-wide license to publish or reproduce the published form of this manuscript, or allow others to do so, for United States Government purposes.

DISCLAIMER

This report was prepared as an account of work sponsored by an agency of the United States Government. Neither the United States Government nor any agency thereof, nor any of their employees, nor any of their contractors, subcontractors, or their employees, makes any warranty, express or implied, or assumes any legal liability or responsibility for the accuracy, completeness, or any third party's use or the results of such use of any information, apparatus, product, or process disclosed, or represents that its use would not infringe privately owned rights. Reference herein to any specific commercial product, process, or service by trade name, trademark, manufacturer, or otherwise, does not necessarily constitute or imply its endorsement, recommendation, or favoring by the United States Government or any agency thereof or its contractors or subcontractors. The views and opinions of authors expressed herein do not necessarily state or reflect those of the United States Government or any agency thereof.

Hydrothermal Growth of ZnO Nanowire Arrays: Fine Tuning by Precursor Supersaturation[†]

Danhua Yan,^{a,b} Jiajie Cen,^b Wenrui Zhang,^a Alexander Orlov,^b and Mingzhao Liu ^{*,a}

Here we develop a technique that fine tunes the hydrothermal growth of ZnO nanowires, to address the difficulties for such controlling in conventional one-pot hydrothermal method. In our technique, precursors are separately and slowly supplied with the assist of a syringe pump, through the entire course of the growth. Comparing to the one-pot method, the significantly lowered supersaturation of precursors helps eliminating competitive homogeneous nucleation and improves the reproducibility. The supersaturation degree can be readily tuned by precursor quantity and injection rate, thus forming ZnO nanowire arrays of various geometry and packing density in a highly controllable fashion. The precise control of ZnO nanowire growth enables systematical studies on the correlation between the material's properties and its morphology. In this work, ZnO nanowire arrays of various morphologies are studied as photoelectrochemical (PEC) water splitting photoanodes, in which we establish clear correlations between the water splitting performance and the nanowires' size, shape, and packing density.

Introduction

Zinc oxide (ZnO), a direct band gap II-IV semiconductor, bears many fascinating properties. With its wide band gap at 3.30 eV ($\lambda = 375$ nm) and large exciton binding energy (60 meV), ZnO enjoys high transparency in visible range and intense band edge luminescence,^{1–6} which enable it for various optical and optoelectronics applications, such as light-emitting diodes, photodetectors, and optical modulator waveguides.^{7–11} Due to its relatively high electron mobility ($\mu_{e,298K} = 155$ cm²V⁻¹s⁻¹), the material is also a promising host for transparent conductive oxides, such as Al:ZnO and Ga:ZnO.^{1–6,12} ZnO usually crystallizes in a hexagonal wurtzite lattice (space group P6₃mc) that lacks inversion symmetry and gives arise to significant piezoelectricity for application in acoustic wave (SAW) devices, filters, and resonators.^{13–19} Given the high surface energy of its polar (002) facets (normal to the hexagonal *c*-axis), wurtzite ZnO readily forms whiskers or nanowires extending along its *c*-axis to minimize the exposed area of (002) facets. In its nanowire form, ZnO finds even more use in applications such as UV lasing, dye-sensitized solar cell, and photoelectrochemical (PEC) water splitting.^{20–24}

A large number of routes have been developed for fabricating ZnO nanowires, using techniques such as vapour-liquid-solid

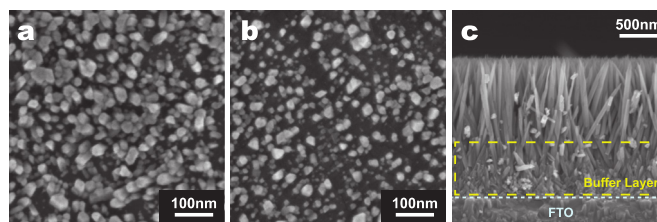


Fig. 1 Limitations of conventional one-pot technique for ZnO nanowires growth. (a)(b) Top-view SEM images for two batches of ZnO nanowires grown from identical *low pH* one-pot process using HMTA as OH⁻ precursors, both with 20 minutes growth time, showing significant morphology variation between the two. (c) Side-view SEM image for ZnO nanowires grown from *high pH* one-pot process using Zn(OH)₄²⁻ as the sole precursors. A densely packed buffer layer emerges between the nanowire array and the substrate.

(VLS) method, molecular beam epitaxy (MBE), pulsed laser deposition (PLD), or metal organic chemical vapour deposition (MOCVD).^{5,16,17,25,26} Among these techniques, the most commonly used one is the seeded hydrothermal growth method developed by Greene et al.^{27–33} In the growth process, substrates seeded with ZnO nanocrystals are submerged into an aqueous solution of zinc ions, which decomposes upon heating (70–90°C), following $\text{Zn}^{2+} + 2\text{OH}^- = \text{ZnO} + \text{H}_2\text{O}$ to form ZnO nanowires over the seeds.^{30,34,35} Employing very simple experimental apparatus and technique, the method is widely adapted and is promising for scalable production of ZnO nanowire arrays. To provide the hydroxide ions while preventing the precipitation of zinc hydroxide, the precursor is commonly a pH neutral solution of zinc salt and hexamethylenetetramine (HMTA), of which the latter slowly decomposes to release hydroxide ions (*low pH* recipe).^{29,32} In

^a Center for Functional Nanomaterials, Brookhaven National Laboratory, Upton, New York 11973, USA. E-mail: mzliu@bnl.gov

^b Department of Materials Science and Engineering, Stony Brook University, Stony Brook, New York 11794, USA

[†] Electronic Supplementary Information (ESI) available: inconsistencies of one-pot hydrothermal growth; packing density of ZnO nanowires; UV-Vis spectroscopy method for nanoscale materials; multiple linear regression results for relationship between nanowire geometry and photocurrent. See DOI: 10.1039/b000000x/

another variation, zinc ions are stabilized in a higher pH (> 13) solution in the form of tetrahydroxozincate ($\text{Zn}(\text{OH})_4^{2-}$), which decomposes to form ZnO upon heating (*high pH* recipe).

As a one-pot method, the technique is simple and effective, but frequently suffers from difficulties in consistency and controllability. As shown in Figure 1a and b, two ZnO nanowire samples grown from an identical *low pH* recipe appear very different on the sizes and packing densities of ZnO deposits, although the only difference is that the two batches were prepared a few days apart. The lacking of consistency is mainly due to the transient nature of the supersaturated precursor solution, i.e., it must be prepared at room temperature and later heated to the growth temperature, which takes about 20 minutes (ESI, Fig.S1a†). Since the precursor decomposition starts gradually as the solution heats up, it is difficult to control the exact reaction starting point, particularly with the temperature inhomogeneity and turbulent convection inside the solution. The situation is aggravated by the method's one-pot nature, i.e., all the precursors are introduced at the very beginning. The high level of supersaturation not only triggers very fast nanowire growth but also makes the competitive homogeneous nucleation the dominant process, as evident by the quick formation of ZnO precipitation (ESI, Fig.S1b†). The growth "burst" at beginning may also lead to very dense nanowires, where many of them cannot extend to full length due to geometrical constraint but instead form a thick "buffer layer", which is especially significant for the *high pH* recipe (Figure 1c).³² Containing numerous randomly oriented crystal domains and grain boundaries, the buffer layer introduces large number of defects that are undesired for applications related to the nanowires' electronic transport properties. To date various attempts have been made to improve the original method, such as using buffer agents including NH_4OH or polyethyleneimine (PEI) to slow down the homogeneous nucleation,^{29,32,33,36,37}. However a method that offers full controllability and tunability to ZnO nanowires growth is yet to be developed.

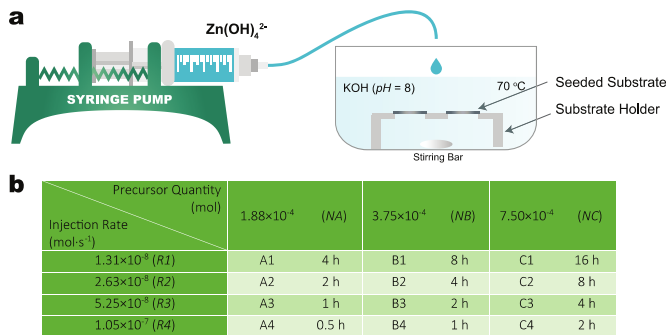


Fig. 2 Experimental set-up for the syringe pump assisted hydrothermal growth (SP) method and summary of growth conditions. (a) The reaction vessel that contains the substrates and reaction medium (100 mL KOH solution at pH 8) is first heated to reaction temperature. The precursor, a 5 mL solution of $\text{Zn}(\text{OH})_4^{2-}$ at various concentration is then loaded into a syringe and pumped into the reaction vessel through a capillary tube, at various pre-set injection rate. (b) Samples are named accordingly to their growth conditions, i.e., precursor quantity and injection rate. The total time for each sample is listed following the sample name.

Here we report a fabrication method that significantly improves the consistency and tunability of the hydrothermal growth of ZnO nanowires, with the assistance of a syringe pump (SP method). In the method a solution of $\text{Zn}(\text{OH})_4^{2-}$ is used as the sole precursor, which is separately stored at room temperature and pumped into the preheated growth bath at a desired uniform rate, thus precisely defining the reaction starting point and guarantees a steady reaction temperature (Figure 2a). As the precursor is pumped in slowly and consumed relatively quickly, the precursor supersaturation is maintained at a relatively low level, which largely suppresses the undesired homogeneous nucleation and helps eliminating the "buffer layer". The consistency and tunability enable the synthesis of ZnO nanowires with various sizes and packing densities at comparable quality, which offers a unique opportunity to systematically study the material's properties versus its morphology. For example, ZnO nanowire arrays are known for decent performance in supporting photoelectrochemical (PEC) water splitting,²¹ however it is not well studied how the performance relates to their morphology. In this work we systematically study the water splitting activities for various ZnO nanowire arrays and discover strong correlations with the nanowires' individual and collective morphology, thus establishing an instructive guideline for designing ZnO nanowire arrays for optimized performance in such applications.

Results and Discussion

ZnO nanowires arrays are fabricated with various experimental parameters to establish the relationship between growth conditions and nanowires morphology. All the ZnO nanowire samples are grown over conductive fluorine-doped tin oxide (FTO) coated glass substrates ($12 \sim 14 \Omega/\text{sq}$) for later PEC water splitting measurements. Prior to the growth a thin layer ($\sim 5 \text{ nm}$) of nanocrystalline ZnO is deposited over the substrates as the seeds, using pulsed laser deposition (PLD). The seeded substrates are then placed into the preheated growth bath ($70 \text{ }^\circ\text{C}$), which contains no precursor but 100 mL of $1 \mu\text{M}$ KOH solution ($\text{pH} = 8$). Two major growth parameters, the total precursor quantity and the injection rate, are investigated. The total precursor quantity is defined as the total molar amount of injected $\text{Zn}(\text{OH})_4^{2-}$ precursor, with the total injection volume fixed at 5 mL. The injection rate, on the other hand, is controlled by the total time taken to inject the 5 mL precursor solution. In the work we study three different precursor quantities, namely $NA = 1.88 \times 10^{-4} \text{ mol}$, $NB = 3.75 \times 10^{-4} \text{ mol}$, and $NC = 7.50 \times 10^{-4} \text{ mol}$, as well as four different injection rates, namely $R1 = 1.31 \times 10^{-8} \text{ mol}\cdot\text{s}^{-1}$, $R2 = 2.63 \times 10^{-8} \text{ mol}\cdot\text{s}^{-1}$, $R3 = 5.25 \times 10^{-8} \text{ mol}\cdot\text{s}^{-1}$, and $R4 = 1.05 \times 10^{-7} \text{ mol}\cdot\text{s}^{-1}$. The twelve samples are named accordingly and are listed in Figure 2b. For instance, sample B3 is grown with precursor quantity NB and injection rate R3. The total reaction time is also listed for each sample.

In general, the SP method produces ZnO crystals in a nanowire shape extruding from the substrate along the *c*-axis, which is identical to ZnO nanowires grown from the one-pot methods (Figure 4).²⁷⁻³³ The growth direction is confirmed by their X-ray diffraction patterns (Figure 3b) in which the diffraction from (002) planes is the strongest. Since the nanowires are not perfectly per-

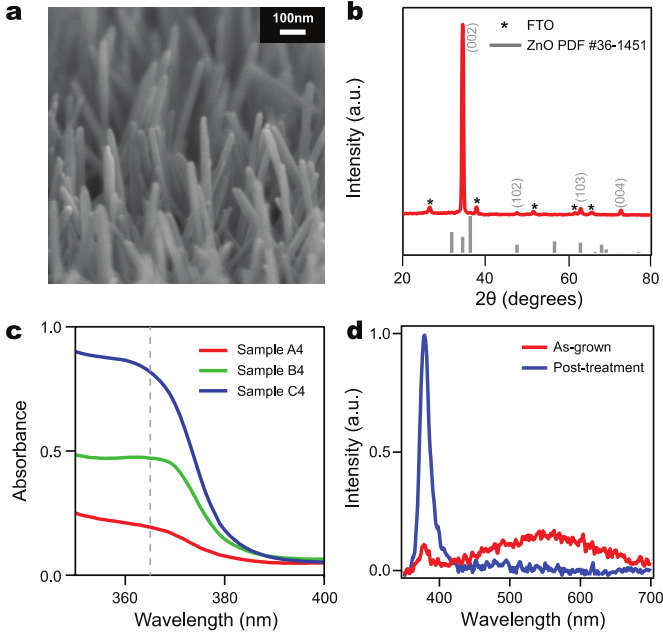


Fig. 3 Structural and optical characterizations of ZnO nanowires. (a) Tilted-view SEM of sample C4, showing nanowires are not perfectly perpendicular to the substrate. (b) X-ray diffraction pattern of ZnO nanowires (sample C4) on FTO substrate. The strongest diffraction from (002) planes indicates that the nanowires grow along its c -axis. (c) Optical absorbance spectra of sample set R4 (sample A4, B4 and C4) with diffuse reflectance corrected by Eq. 3 (ESI, Fig.S3†). (d) PL spectra of the ZnO nanowire array before (red line) and after (blue line) post-treatment to remove deep hole traps.

pendicular to the substrate (Figure 3a), diffractions from other lattice planes appear in weaker peaks. As-grown ZnO nanowires contains large amount of deep hole traps, represent in the steady state photoluminescence (PL) spectra as a weak band gap emission near 3.3 eV (376 nm) and a stronger deep-level emission at 2.2 eV (560 nm) (Figure 3d). We follow a post-treatment procedure reported previously to remove these deep hole traps and defects.²¹ After the treatment, the band gap emission is greatly enhanced and the deep-level emission is suppressed, suggesting the successful removal of these deep hole traps. Significant variation in morphologies is observed for ZnO nanowires grown under different conditions, as shown by their scanning electron microscopy (SEM) images (Figure 4). At a fixed total precursor quantity, the precursor injection rate has a great impact on the nanowire length, diameter and packing density. For the cases of lower total precursor quantity (NA and NB), a higher precursor injection rate produces nanowires of lower aspect ratio but higher packing density (Figure 4, top-view SEM images in ESI, Fig.S2†). The total quantity of precursor impacts the nanowire morphology as well. At the same injection rate, larger precursor quantity typically produces longer and thicker nanowires, due to its longer growth time (Figure 2b). However, these trends do not hold very consistently at the largest precursor quantity, *i.e.*, the sample set NC . For example, Sample C1 features very short nanowires despite its low injection rate and long growth time, which deviates from the established trends significantly (Figure 4). The devia-

tion is likely due to the fact that NC involves a precursor solution of much higher concentration (0.15 M). When injected into the growth solution, the high local precursor concentration promotes homogeneous nucleation and generates large amount of ZnO precipitates. The aggravated homogeneous nucleation thus leaves less precursor molecules available for seeded growth over the substrates. In this sense, the sample set NC is similar to the one-pot method, in which higher precursor concentration makes homogeneous nucleation the dominant process and makes the nanowires growth less controllable.

The morphology of a ZnO NWs array is quantitatively characterized by the nanowires' mean length \bar{L} , mean diameter \bar{D} , mean aspect ratio \bar{R} , as well as the packing density η defined by the number of nanowires per unit area, which are listed in Table 1 for all twelve samples. The mean length \bar{L} and mean diameter \bar{D} for each sample are obtained by averaging the measurements of 50 nanowires from corresponding side-view SEM images, while the mean aspect ratio \bar{R} equals \bar{L}/\bar{D} . The packing density η is determined by optical absorption spectroscopy, taking advantage of the strong band edge absorption of ZnO (Figure 3c). At wavelength λ , the nanowire array's spectral absorbance $A(\lambda)$ is given by the Lambert-Beer Law:

$$A(\lambda) = \varepsilon(\lambda)cl \quad (1)$$

where ε is the molar extinction coefficient of *bulk* ZnO, c the volume fraction of nanowires, and l the optical path length. Considering that $c = \bar{v}\eta/l$, where $\bar{v} = (\pi D^2 L/4)$ is the nanowire mean volume, Eq. 1 readily rewrites:

$$A(\lambda) = \varepsilon(\lambda)\bar{v}\eta \quad (2)$$

which establishes a linear relation between η and $A(\lambda)$. Experimentally we obtain spectral absorbance $A(\lambda)$ using:

$$A(\lambda) = \log_{10} \frac{1 - R(\lambda)}{T(\lambda)} \quad (3)$$

where $T(\lambda)$ is the transmittance and $R(\lambda)$ the reflectance (Figure 3c and ESI†). In general, higher spectral absorbance is observed for samples from larger precursor quantity, which reflects the higher volume of ZnO deposition and is consistent with SEM studies (Figure 4). To determine η from Eq. 2 we choose $\lambda = 365$ nm ($\varepsilon_{365} = 8.69 \times 10^4$ cm⁻¹), where the optical absorption of ZnO nanowires is sufficiently strong, yet not too much to undermine the accuracy of transmittance measurement.³⁸

Through the quantitative analysis, the morphology parameters (\bar{L} , \bar{D} , \bar{R} , and η) obtained for different ZnO nanowire arrays are very similar in trend to the qualitative observation from the corresponding SEM images (Figure 5). For samples grown from relatively low precursor quantity (NA and NB), the mean length \bar{L} and aspect ratio \bar{R} are negatively correlated to the injection rate (Figure 5a,b). The trend is consistent with the classical crystal growth theory, in which growth regime evolves with regard to the degree of precursor supersaturation.^{39,40} In the low supersaturation regime that is achieved at lower injection rate, the growth is dominated by deposition over spiral steps around screw dislocations and essentially one-dimensional (1D), follow-

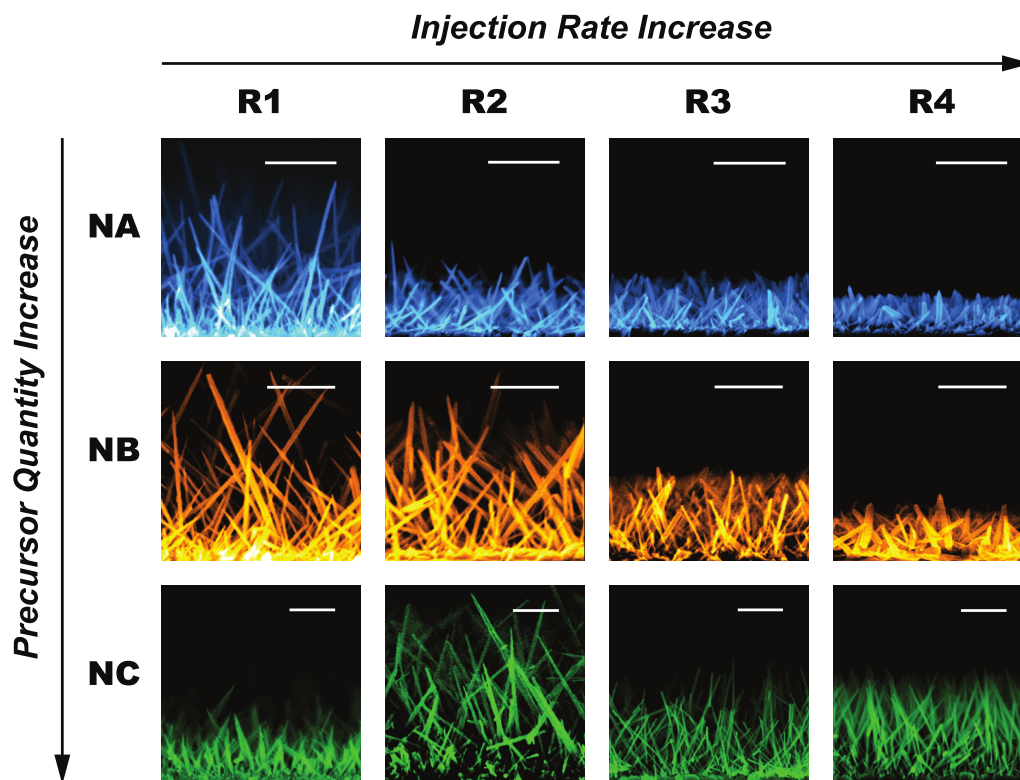


Fig. 4 SEM images of ZnO nanowires prepared under different growth conditions. Both the injection rate and the precursor quantity have a strong impact on the morphology of ZnO nanowires. Growth with larger precursor quantity at higher injection rate typically produce longer, thicker nanowires packed more densely. Scale bar = 500 nm.

ing the Burton-Cabrera-Frank (BCF) mechanism.^{41,42} The regime thus favours the growth of high aspect ratios nanowires, which is consistent with the experimental observation. At higher injection rate, the supersaturation degree increases toward a new regime that favours two-dimensional (2D) nuclei formation over crystal surface. As the 2D nuclei subsequently spread across the surface and coalesce to form layers, the regime is commonly referred as *layer-growth* mechanism.^{40,43} In this regime, the radial growth is less discriminated against the axial growth, thus producing ZnO nanowires of low aspect ratios.⁴⁴ Larger packing density η is also observed for the cases of higher injection rate (Figure 5c), which is due to the smaller critical nucleation size and higher nucleation probability at higher supersaturation degree.⁴⁵ The latter observation echoes the results from the conventional one-pot process, in which very crowded nanowires are formed due to the very high initial precursor concentration. As discussed earlier, over-crowded nanowires are not always desirable for applications related to electronic transports, due to the formation of “buffer layer” that contains numerous grain boundaries and defects.

It is well known that ZnO nanowire array supports photoelectrochemical (PEC) water splitting as a water oxidation photoanode. To date, there are few systematic studies on how the water splitting performance relates to the nanowire array’s morphology. The SP technique developed in this work offers the required tunability and consistency to fabricate ZnO nanowires of desired dimensions and packing density, so that we can quantitatively corre-

late the water splitting activities against the nanowire array morphology. The water splitting activities are assessed by measuring the photocurrent density (J) versus electrode potential (E) under AM 1.5G illumination (6). The photocurrent densities at the thermodynamic potential of oxygen evolving (1.23 V_{RHE} at 25 °C) are summarized in Figure 6b for all the samples. In general, among each sample set of identical precursor quantity, the largest photocurrent density is always observed from ZnO nanowire arrays prepared at the highest precursor injection rate, e.g., samples A4, B4 and C4, which have the lowest aspect ratio and the highest packing density among their respective set. On the other hand, when compared between ZnO nanowire arrays grown under identical precursor injection rate, larger photocurrent is typically observed from the one produced with higher precursor quantity, which features thicker and longer nanowires for more effective light absorption.

Considering the variation of nanowire packing density η across different samples, a more accurate comparison is made by normalizing the photocurrent density J against η to obtain photocurrent per nanowire $i = J/\eta$, under AM 1.5G radiation. The normalized photocurrent i thus only depends on the size and shape of individual ZnO nanowire, namely its length L and diameter D . As shown in Figure 6c and Figure 6d, the normalized photocurrent has strong positive correlations with both nanowire length L and diameter D . To quantify the correlation, we assume an empirical relationship between i and geometry parameters L and

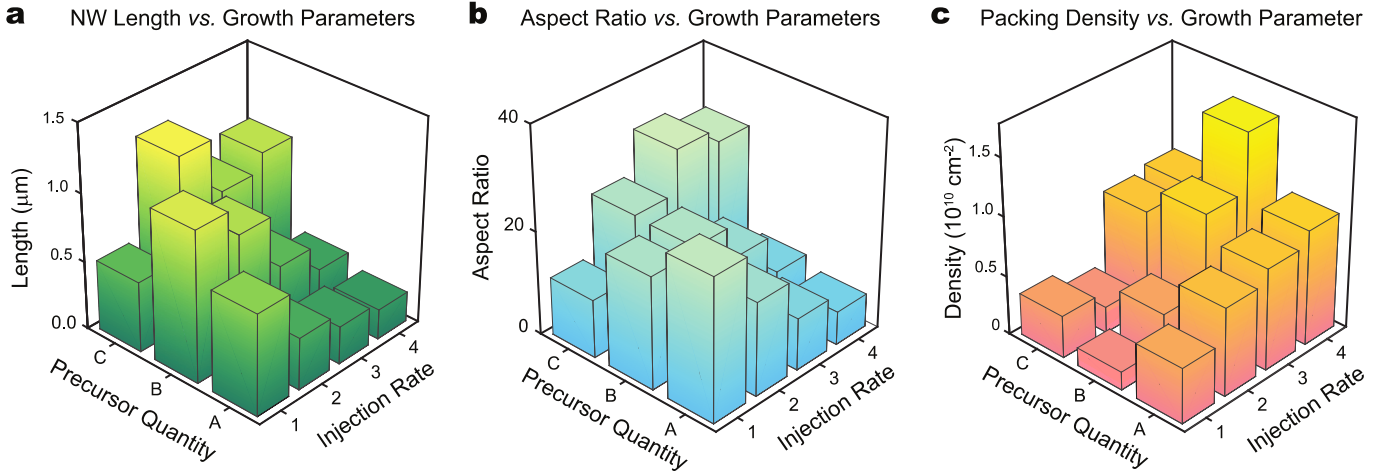


Fig. 5 The correlation between growth conditions and ZnO nanowires morphology in various aspects: (a) Mean nanowire length \bar{L} , (b) mean aspect ratio \bar{R} , and (c) packing density η .

Table 1 Summary of morphology parameters for all twelve samples: length (\bar{L}), diameter (\bar{D}), aspect ratio (\bar{R}), and packing density (η) calculated by corresponding absorbance for each sample.

Sample Name	Mean Length \bar{L} (nm)	Mean Diameter \bar{D} (nm)	Aspect Ratio \bar{R}	Packing Density η (cm ⁻²)
A1	$7.43 \pm 2.85 \times 10^2$	27.0 ± 8.3	27.6	1.86×10^9
A2	$3.82 \pm 1.30 \times 10^2$	21.2 ± 4.7	18.0	2.96×10^9
A3	$2.77 \pm 0.88 \times 10^2$	27.6 ± 7.0	10.0	3.42×10^9
A4	$2.19 \pm 0.39 \times 10^2$	34.2 ± 7.1	6.4	3.87×10^9
B1	$1.11 \pm 0.46 \times 10^3$	51.1 ± 10.7	21.7	6.12×10^8
B2	$9.04 \pm 2.47 \times 10^2$	40.0 ± 9.5	22.6	1.69×10^9
B3	$5.02 \pm 1.23 \times 10^2$	31.0 ± 11.1	16.2	4.23×10^9
B4	$3.02 \pm 0.66 \times 10^2$	35.7 ± 8.9	8.4	6.17×10^9
C1	$5.16 \pm 2.12 \times 10^2$	46.0 ± 11.2	11.2	1.42×10^9
C2	$1.25 \pm 0.46 \times 10^3$	54.8 ± 15.0	22.9	8.81×10^8
C3	$8.45 \pm 2.12 \times 10^2$	27.2 ± 7.0	31.1	3.35×10^9
C4	$9.71 \pm 2.59 \times 10^2$	34.2 ± 7.9	28.4	3.53×10^9

D:

$$i = kL^m D^n \quad (4)$$

where k , m and n are empirical coefficients. The exponent factors m and n are determined through a multiple linear regression on the logarithm form of Eq. 4, $\ln i = \ln k + m \ln L + n \ln D$, which gives $m = 0.48$ and $n = 1.80$ with $R^2 = 0.9$ and $p < 0.01$ (ESI[†]), i.e.:

$$i \propto L^{0.48} D^{1.80}. \quad (5)$$

The result has a few implications. First of all, the exponent factor for diameter, n , is very close to 2, indicating that the normalized photocurrent i is proportional to the nanowire's radial cross-sectional area. As the nanowires are nearly vertical, it suggests that i is directly proportional to the nanowire's optical absorption cross-section and that the nanowires have very similar charge carrier separation efficiency regardless of their diameters. Secondly, the nanowire length L is apparently playing a less significant role here, with an exponent factor of only ~ 0.5 . It reflects that, despite that longer nanowires produce more effective optical absorption, the effect is limited due to light attenuation along

axial direction of the nanowire. Hence it can be inferred from Eq. 5 that for the same volume, shorter but thicker nanowire would be favoured for higher photocurrent, which is consistent with our qualitative observations. This trend is more explicitly demonstrated by realizing that the nanowire volume $v = \pi L D^2 / 4$ and that the aspect ratio $R = L / D$, so that the empirical relation in Eq. 5 rewrites:

$$i \propto v^{0.76} R^{-0.28} \quad (6)$$

At such, it becomes very clear that higher photocurrent is achieved by larger nanowires of lower aspect ratio, for the range of nanowire dimensions studied here, i.e., diameter D from 20 to 60 nm and length L from 0.3 to 1.2 μm .

One may note that the photocurrent, normalized or not, is not the sole gauge of the water splitting activity for a nanowire array photoelectrode. Other important gauges include its photocurrent onset potential and its J - E characteristics near the onset. Across the entire sample sets, we find that they all have very similar onset potential at about 0.4 V_{RHE}, but quite different J - E characteristics near the onset. Taking the example of sample set R4 (Figure 6a),

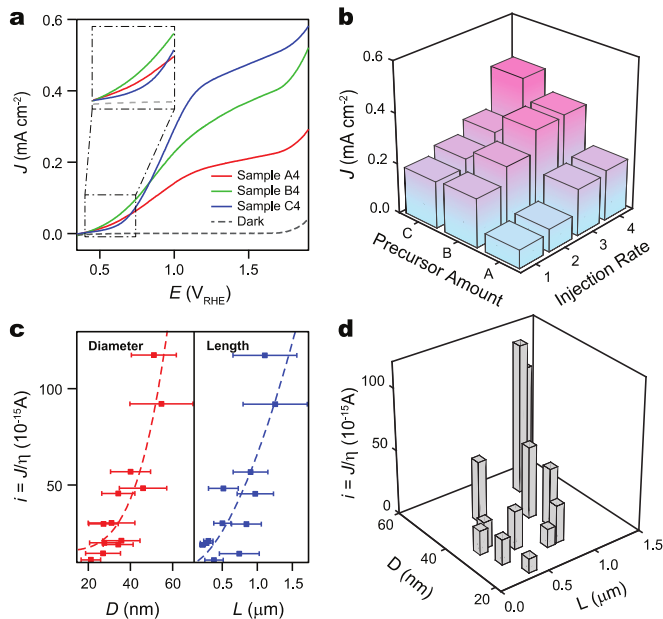


Fig. 6 The PEC water splitting performance of the ZnO nanowire arrays and its correlation with sample morphology. (a) Photocurrent curve vs. potential curves for sample set R4, and sample C4 behaves differently from sample A4 and B4 near the onset potential, and voltage range from $0.4 V_{\text{RHE}}$ to $0.8 V_{\text{RHE}}$ is enlarged (inset) for a clearer view. (b) Photocurrent density at $1.23 V_{\text{RHE}}$ (the thermodynamic potential for oxygen evolving at 25°C) under AM 1.5G illumination for each sample. (c) Both mean diameter and length for a nanowire is strongly positively correlated to the normalized photocurrent, showing the validity of fitting these values into a multiple regression model. (d) Normalized photocurrent i for a single nanowire exhibits strong correlation with both nanowire diameter and length.

in which each sample has the best photocurrent among the group, sample C4 clearly has a PEC behaviour different from those of A4 and B4. Despite its highest photocurrent at $1.23 V_{\text{RHE}}$, C4 features lower photocurrent near the onset potential than A4 and B4 (Figure 6a inset). The observation suggests that C4 suffers from a more severe charge carrier recombination that is only overcome at more anodic potentials. Given that C4 are grown very rapidly with high precursor injection rate, it is prone to increased defects formation between substrate and nanowires, which leads to less effective charge carrier separation at lower potentials.

Conclusion

In summary, the syringe pump method developed in this work features high controllability and tunability for the geometry of the ZnO nanowire array, significantly improves the consistency and reproducibility for ZnO nanowires growth over the traditional one-pot hydrothermal growth method. Different aspect ratios of ZnO nanowires are achieved by fine tuning the supersaturation degree in precursor solution, which is representing different growth regimes for ZnO crystals, from axial one-dimensional growth (*high aspect ratio* nanowire) to radial two-dimensional growth (*low aspect ratio* nanowire). Besides, various packing densities for ZnO nanowire arrays can also be tuned *via* different supersaturation degrees, for higher supersaturation favors smaller

critical nucleation size and higher nucleation probability, leading to an increased packing density for nanowire arrays. As such, ZnO nanowire arrays of desired morphology can be fabricated for numerous applications throughout optical, electrical, or mechanical engineering research fields. Here, by taking advantages of such controllability, we demonstrate that the relationship between the nanowire morphology and the photoelectrochemical (PEC) water splitting performance can be explicitly revealed. Finally, hydrothermal growth has been widely adapted for the synthesis of a variety of metal oxide nanowire arrays beyond ZnO, such as TiO_2 , BaTiO_3 , and lead zirconate titanate (PZT).⁴⁶⁻⁴⁸ The high reproducibility and capability for fine tuning offered by the syringe pump technique sheds a new light for significantly improving this already powerful technique.

Methods

Fabricating of ZnO nanowire array photoelectrodes

The syringe pump assisted hydrothermal growth method (SP method) is employed for fabricating ZnO nanowires over fluorine-doped tin oxide (FTO) coated glasses (MTI Corporation, $12\sim 14 \Omega/\text{sq}$).²⁷ All the FTO substrates are cleaned consecutively in acetone, ethanol and deionized water (DI water) at room temperature under sonication for 2 minutes each. Prior to seeding process they are further cleaned in an oxygen plasma. ZnO seeding layer is deposited onto FTO substrate by pulsed layer deposition (PLD, PVD Products PLD/MBE 2300) at room temperature for 500 pulses at 5 Hz ($\sim 3 \text{ nm}$). After the deposition, ZnO thin films are annealed in oxygen at 400°C for 10 minutes in a rapid thermal annealer (RTA), to improve the crystallinity of ZnO seeds.

Seeded substrates are first submerged into 100 mL $1 \mu\text{M}$ KOH solution ($\text{pH} = 8$), where OH^- ions are used to buffer the ultra thin ZnO seed layer from dissolving into the DI water. The vessel is then placed into a preheated silicone oil bath and heated to the pre-set 70°C . Once the pre-set temperature is reached, the precursor solution is gradually injected into the growth solution using a syringe pump, through a capillary tube (Figure.2a). The precursor solution is prepared by mixing zinc nitrate and potassium hydroxide at a 1:20 molar ratio to form a clear $\text{Zn}(\text{OH})_4^{2-}$ solution. In all experiments the injected volume is fixed to 5 mL, with different Zn^{2+} concentration and injection rate to produce ZnO nanowires of different morphology. After the growth, all the ZnO nanowires are annealed in oxygen at 500°C for 15 minutes in a rapid thermal annealer (RTA), and then are treated under O_2 plasma for 15 minutes to remove the deep hole traps and defects.

Characterization and Photoelectrochemistry Measurement

Morphologies of ZnO nanowires are studied by scanning electron microscopy (SEM, Hitachi S4800). X-Ray diffraction (XRD, Rigaku Ultima III) is conducted to confirm the formation and crystalline of ZnO nanowires. Optical absorption of ZnO nanowires are determined by measuring the UV-vis optical transmission and diffused reflection spectra using an integrating sphere (Perkin Elmer Lambda 950) (ESI[†]). Photoluminescence spectra of the nanowire arrays are measured in an ISS PC1/K2 spectrofluorometer that uses a xenon lamp for optical excitation and a photon

multiplier tube for PL detection. The excitation wavelength is set to 280 nm by a monochromator at the normal direction to the excitation beam. A 350 nm long-pass filter is inserted between the sample and the second filter is inserted between the sample and the second monochromator to remove the scattered excitation light. The PEC water splitting performance of ZnO nanowire arrays are measured by a potentiostat (VersaStat4, PAR), using a three-electrode PEC cell under illumination of a 150 W solar simulator with an AM 1.5G filter (Newport). The ZnO nanowire array is used as the working electrode with an active illumination area of 1.0 cm², with a platinum wire as the counter electrode, an Ag|AgCl|3 M KCl electrode as the reference electrode (0.1941 V_{NHE} at 25 °C), and a 0.1 M KOH solution (pH = 13) solution as the electrolyte. The potential recorded experimentally, $E_{\text{AgCl/Ag}}$, is converted to a potential in reference of the reversible hydrogen electrode (RHE), E_{RHE} , according to the Nernst equation:

$$E_{\text{RHE}} = E_{\text{AgCl/Ag}} + E_{\text{AgCl/Ag}}^{\circ} + 0.05917\text{pH} \quad (7)$$

where the E_{RHE} is the potential converted, $E_{\text{AgCl/Ag}}$ is the potential measured, $E_{\text{AgCl/Ag}}^{\circ} = 0.1941 \text{ V}_{\text{NHE}}$ at 25 °C, and pH = 13 in our case. The incident light power is calibrated before each measurement, using a calibrated quartz-windowed silicon solar cell (Newport) and a spectrometer (Ocean Optics) as described in previously reports.^{21,49}

Acknowledgements

This research used resources of the Center for Functional Nanomaterials, which is a U.S. DOE Office of Science Facility, at Brookhaven National Laboratory under Contract No. DE-SC0012704.

References

- 1 K. Appavoo, M. Liu and M. Y. Sfeir, *Appl. Phys. Lett.*, 2014, **104**, 133101.
- 2 S. Guillemin, V. Consonni, E. Appert, E. Puyoo, L. Rapenne and H. Roussel, *J. Phys. Chem. C*, 2012, **116**, 25106–25111.
- 3 M. Guptaand, V. Sharma, J. Shrivastava, A. Solanki, a. P. Singh, V. R. Satsangi, S. Dass and R. Shrivastav, *Bull. Mater. Sci.*, 2009, **32**, 23–30.
- 4 Y. Hu, X. Yan, Y. Gu, X. Chen, Z. Bai, Z. Kang, F. Long and Y. Zhang, *Appl. Surf. Sci.*, 2015, **339**, 122–127.
- 5 R. C. Pawar, J. S. Shaikh, a. a. Babar, P. M. Dhere and P. S. Patil, *Sol. Energy*, 2011, **85**, 1119–1127.
- 6 L. Qin, C. Shing, S. Sawyer and P. S. Dutta, *Opt. Mater.*, 2011, **33**, 359–362.
- 7 R. N. Koch, M H; Timbrel, P Y; Lamb, *Semicond. Sci. Technol.*, 1995, **10**, 2–7.
- 8 Y. Chen, D. Bagnall and T. Yao, *Mater. Sci. Eng., B*, 2000, **75**, 190–198.
- 9 N. Saito, H. Haneda, T. Sekiguchi, N. Ohashi, I. Sakaguchi and K. Koumoto, *Adv. Mater.*, 2002, **14**, 418–420.
- 10 S. Liang, H. Sheng, Y. Liu, Z. Huo, Y. Lu and H. Shen, *J. Cryst. Growth*, 2001, **225**, 110–113.
- 11 J. Y. Lee, Y. S. Choi, J. H. Kim, M. O. Park and S. Im, *Thin Solid Films*, 2002, **403-404**, 553–557.
- 12 H. Tang, K. Prasad, R. Sanjin s, P. E. Schmid and F. L. vy, *J. Appl. Phys.*, 1994, **75**, 2042.
- 13 N. Golego, S. A. Studenikin and M. Cocivera, *J Electrochem Soc*, 2000, **147**, 1592–1594.
- 14 N. Emanetoglu, C. Gorla, Y. Liu, S. Liang and Y. Lu, *Mater. Sci. Semicond. Process.*, 1999, **2**, 247–252.
- 15 Y. Lin, Z. Zhang, Z. Tang, F. Yuan and J. Li, *Adv. Mater. Opt. Electron.*, 1999, **9**, 205–209.
- 16 J. H. Choi, H. Tabata and T. Kawai, *J. Cryst. Growth*, 2001, **226**, 493–500.
- 17 P. Yang, H. Yan, S. Mao, R. Russo, J. Johnson, R. Saykally, N. Morris, J. Pham, R. He and H.-J. Choi, *Adv. Funct. Mater.*, 2002, **12**, 323–331.
- 18 E.-C. Lee and K. J. Chang, *Phys. Rev. B*, 2004, **70**, 115210.
- 19 Q. Li, V. Kumar, Y. Li, H. Zhang, T. J. Marks and R. P. H. Chang, *Chem. Mater.*, 2005, **17**, 1001–1006.
- 20 M. D. McCluskey and S. J. Jokela, *J. Appl. Phys.*, 2009, **106**, 1–14.
- 21 M. Liu, C. Y. Nam, C. T. Black, J. Kamcev and L. Zhang, *J. Phys. Chem. C*, 2013, **117**, 13396–13402.
- 22 R. Amiruddin, S. Devasia, D. K. Mohammedali and M. C. Santhosh Kumar, *Semicond. Sci. Technol.*, 2015, **30**, 035009.
- 23 K. S. Ahn, Y. Yan, S. Shet, T. Deutsch, J. Turner and M. Al-Jassim, *Appl. Phys. Lett.*, 2007, **91**, 17–19.
- 24 H. Li, Y. Fu, H. Liu, M. Zhu, Z. Peng, J. Yang, J. Li, X. Huang, Y. Jiang, Q. Liu, X. Shi, H. Wu, Y. Yang and Q. Liu, *Inorg. Chem. Commun.*, 2013, **30**, 182–186.
- 25 Z. W. Pan, Z. R. Dai and Z. L. Wang, *Science (New York, N.Y.)*, 2001, **291**, 1947–1949.
- 26 T. Zhang, W. Dong, M. Keeter-Brewer, S. Konar, R. N. Njabon and Z. R. Tian, *J. Am. Chem. Soc.*, 2006, **128**, 10960–10968.
- 27 L. E. Greene, M. Law, J. Goldberger, F. Kim, J. C. Johnson, Y. Zhang, R. J. Saykally and P. Yang, *Angew. Chem. Int. Ed.*, 2003, **42**, 3031–3034.
- 28 H. S. Jang, B. Son, H. Song, G. Y. Jung and H. C. Ko, *J. Mater. Sci.*, 2014, **49**, 8000–8009.
- 29 K. M. McPeak, T. P. Le, N. G. Britton, Z. S. Nickolov, Y. a. Elabd and J. B. Baxter, *Langmuir*, 2011, **27**, 3672–3677.
- 30 V. F. Rivera, F. Auras, P. Motto, S. Stassi, G. Canavese, E. Celasco, T. Bein, B. Onida and V. Cauda, *Chem. Eur. J.*, 2013, **19**, 14665–14674.
- 31 L. Vayssieres, *Adv. Mater.*, 2003, **15**, 464–466.
- 32 C. Xu, P. Shin, L. Cao and D. Gao, *J. Phys. Chem. C*, 2010, **114**, 125–129.
- 33 Y. Zhou, W. Wu, G. Hu, H. Wu and S. Cui, *Mater. Res. Bull.*, 2008, **43**, 2113–2118.
- 34 L. E. Greene, M. Law, D. H. Tan, M. Montano, J. Goldberger, G. Somorjai and P. Yang, *Nano Lett.*, 2005, **5**, 1231–1236.
- 35 L.-W. Ji, S.-M. Peng, J.-S. Wu, W.-S. Shih, C.-Z. Wu and I.-T. Tang, *J. Phys. Chem. Solids*, 2009, **70**, 1359–1362.
- 36 Y. Tak, D. Park and K. Yong, *J. Vac. Sci. Technol., B: Microelectron. Nanometer Struct.*, 2006, **24**, 2047.
- 37 M. Law, L. E. Greene, J. C. Johnson, R. Saykally and P. Yang,

- Nat. Mater.*, 2005, **4**, 455–459.
- 38 H. Yoshikawa and S. Adachi, *Jpn. J. Appl. Phys.*, 1997, **36**, 6237–6243.
- 39 D. P. Woodruff, *Philos. Trans. R. Soc., A*, 2015, **373**, 1–11.
- 40 J. Cejka, A. Corma and S. Zones, *Zeolites and catalysis: synthesis, reactions and applications*, John Wiley & Sons, 2010.
- 41 F. C. Frank, *Discuss. Faraday Soc.*, 1949, **5**, 48.
- 42 W. K. Burton, N. Cabrera and F. C. Frank, *Philos. Trans. R. Soc., A*, 1951, **243**, 299–358.
- 43 v.-W. Kossel, *Ann. Phys.*, 1934, **413**, 457–480.
- 44 S. A. Morin, M. J. Bierman, J. Tong and S. Jin, *Science (New York, N.Y.)*, 2010, **328**, 476–480.
- 45 D. Kashchiev and G. M. van Rosmalen, *Cryst. Res. Technol.*, 2003, **38**, 555–574.
- 46 D.-D. Qin, Y.-P. Bi, X.-J. Feng, W. Wang, G. D. Barber, T. Wang, Y.-M. Song, X.-Q. Lu and T. E. Mallouk, *Chem. Mater.*, 2015, **27**, 4180–4183.
- 47 Y. Lin, Y. Liu and H. A. Sodano, *Appl. Phys. Lett.*, 2009, **95**, 2901.
- 48 U. A. Joshi, S. Yoon, S. Baik and J. S. Lee, *J. Phys. Chem. B*, 2006, **110**, 12249–12256.
- 49 D. Yan, J. Tao, K. Kisslinger, J. Cen, Q. Wu, A. Orlov and M. Liu, *Nanoscale*, 2015, **7**, 18515–18523.